ACS OMEGA

Open Access

http://pubs.acs.org/journal/acsodf

Article

Numerical Approximation of a Nonequilibrium Model of Gradient Elution Chromatography Considering Different Functional Relationships between Model Parameters and Solvent Composition

Arif Mahmood, Muhammad Uzair, Sadia Perveen,* Nazia Rehman, and Shamsul Qamar

Cite This: *ACS Omega* 2024, 9, 20601−20615

Read Online

ACCESS | Metrics & More | Article Recommendations

ABSTRACT: In this paper, a rigorous theoretical study is conducted to analyze the influence of varying solvent compositions on the retention characteristics of elution profiles within a fixed-bed liquid chromatographic column. In gradient chromatography, the propagation speed of elution profiles is manipulated through a progressive variation in the mobile-phase composition. Consequently, enhanced separation of the mixture components can be achieved together with a reduction in the requisite recycling times for subsequent injections. In other words, both the efficiency and the selectivity of the column can be enhanced. The lumped kinetic model coupled with the convection−diffusion equation for the volume fraction of the solvent is applied to simulate the process. The resulting nonlinear model equations are numerically solved by applying a semidiscrete second-order finite-volume method. The numerical solutions are utilized to quantify the effects of gradient starting and ending times, solvent composition, solvent strength parameters, and gradient slope on the concentration profiles. Additionally, temporal numerical moments are plotted versus the starting and ending times of the gradient, and standard performance criteria are presented for evaluating the process performance. The outcomes of this investigation will contribute to further enhancements in gradient elution chromatography.

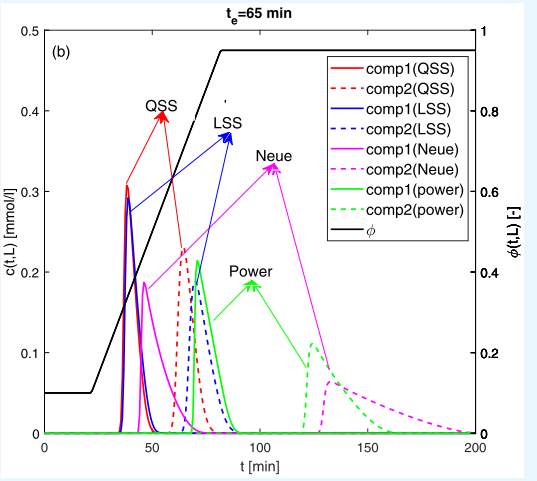

1. INTRODUCTION

Gradient elution chromatography is a sophisticated and highly efficient technique widely utilized in the separation of complex mixtures of chemical compounds, especially when the components exhibit a broad spectrum of polarities and molecular weights. The foundational principles of gradient elution chromatography were established approximately 50 years ago.[1,2] Owing to its unceasing and extensive utilization in the domain of separation sciences, gradient elution chromatography has been persistently reviewed, debated, and enhanced up to the present day. This ongoing refinement underscores its pivotal role and enduring relevance in facilitating intricate separation tasks, marking its prominence in both academic and industrial settings. The evolution of this technique is characterized by systematic improvements, each contributing to augmenting its efficacy, precision, and adaptability to meet the complex demands of contemporary separation challenges.[3,4]

In the process of elution chromatography, a sample mixture is injected into a column that is densely packed with adsorbent particles. This mixture is then transported through the system by a flowing mobile phase, commonly referred to as the eluent. Different components of the mixture bind to the sorbent with varying strengths, causing them to travel at different speeds through the column. As a result, the components are separated and emerge individually at the column's outlet.[5] On the other hand, isocratic elution is a type of chromatography in which the eluent's composition and strength remain constant throughout the separation process. However, this method can be inefficient for mixtures with components exhibiting diverse adsorption behaviors, leading to incomplete separation within a reasonable time frame. A common solution to this issue, particularly in liquid chromatography, is the gradient elution technique. In this approach, the eluent's strength is progressively increased by altering the concentration of solvent.[8] Such a variation in the solvent composition makes possible the separation of all

Received: March 13, 2024
Accepted: April 10, 2024
Published: April 25, 2024

mixture components during a single operation and improves the overall peak capacity of the system, allowing for the resolution of more components within a given time period.[6,7]

The mobile phase in gradient elution chromatography is typically a mixture of two solvents, such as water and acetonitrile. The strength of the mobile phase is determined by the ratio of the two solvents. In gradient elution, the mobile-phase composition is progressively altered throughout the analysis. As a consequence, compounds are eluted from the column sequentially based on their increasing polarity, with less polar compounds eluting earlier, followed by the elution of more polar entities.[9]

Gradient elution chromatography is prevalent in both the analytical and preparative chromatography realms. Within the scope of analytical chromatography, this technique is instrumental in the identification and quantification of specific compounds in mixtures. In the context of preparative chromatography, gradient elution serves as an efficient method for the isolation and purification of distinct compounds from complex mixtures. Various gradient elution profiles can be employed, each tailored to the unique requirements of a particular analysis.[10] Out of them, the linear gradient, in which the mobile-phase composition varies linearly with time, is frequently used.[11−14] Additionally, other gradient types, such as step, concave, and convex gradients, offer alternative approaches to suit specific analytical needs. The selection of a gradient profile is influenced by several factors, encompassing the sample composition, the targeted resolution, and the temporal limitations associated with the analysis.[3,4]

Models based on theoretical frameworks are instrumental for the optimization of gradient elution methodologies and offer predictive insights into the impact of diverse parameters on the separation process. Recent theoretical models for gradient elution have been formulated within a range of linear concentrations, excluding kinetic resistances or mass transfer. Scaling-up procedures for protein purification utilizing gradient elution are predominantly empirical in nature.[15] Mass-transfer resistances are particularly significant for macromolecules. Diverse dispersion phenomena, including axial dispersion, mass-transfer resistances, and slow kinetics, often offset the thermodynamic implications of the adsorption and desorption processes. These effects are influenced by several factors such as the gradient slope, the initial modulator concentration, and the adsorptive characteristics of the eluites and the modulator. Theoretical underpinnings of gradient elution techniques within the realm of nonlinear chromatography are not yet fully formulated.[16]

The conventional model for gradient retention is based on the fact that there is a linear correlation between the logarithm of the retention factor and the composition of solvent. However, numerous experimental and theoretical investigations have contested this assumption, indicating that it is an approximation. In reality, a notable curvature characterizes such relationships, exhibiting an augmentation at lower retention levels in contrast to the expected logarithmic linear correlation.[17,18] Bosch and Roses have advocated for the utilization of a polarity index as a standard for evaluating the strength of elution in a reversed-phase mobile phase.[19−21] It is observed that this index maintains a nonlinear correspondence with the volumetric composition of the solvent. A study conducted by García-Alvarez-Coque et al.[22] provided evidence that supports the superiority of the nonlinear model, proposed by Roses and Bosch, over the classical linear relationship model. The research illustrated that the curved model offers enhanced predictions of the retention of various compounds. Furthermore, it was observed that this model yields improved associations between gradient and isocratic conditions. Nikitas et al.[18,23,24] have introduced more intricate theories concerning retention in reversed-phase chromatography. The researchers have formulated semithermodynamic models[18] for retention in reversed-phase chromatography and conducted comparative analyses of multiple models.[23,24] Their study endorsed an equation that integrates a logarithmic function with a function akin to the polarity index function, initially proposed by Roses and Bosch, affirming it as the most effective retention descriptor. The equation employed by Neue et al.[25] bears significant similarity to the favored equation of Nikitas et al.[18] A nonlinear empirical equation is employed to characterize the association between chromatographic retention and solvent composition, applicable to both isocratic and gradient chromatography as pointed out by Neue and Kuss.[26] The inclination toward curved associations between the logarithmic values of the retention factor and the composition of the solvent is clearly observable, irrespective of whether they are derived theoretically or empirically. Such relationships are deemed to be superior for precise assessments of retention in reversed-phase chromatography.

In this contribution, a lumped kinetic model (LKM) coupled with a convection−diffusion equation for the volume fraction of the solvent is formulated and solved numerically to simulate the gradient chromatography process. The linear solvent strength (LSS) model and various functional relationships between model parameters and solvent composition are taken into consideration. A semidiscrete second-order finite-volume scheme is extended and applied to approximate the resulting nonlinear model equations. The suggested scheme provides second-order accuracy, captures sharp discontinuities, and prevents numerical dissipation.[27−29] The performance of scheme is evaluated in the cases of single-solute and multicomponent mixtures. A comparative analysis with isocratic elution outcomes is also presented. Emphasis is placed on assessing the influence of model parameters on the behavior, propagation speed, and separation of elution profiles. The outcomes of this research work will be helpful for practitioners to optimize and upgrade gradient elution chromatography.

The novelty of this research work includes the following. (1) For the first time, a full LKM is formulated considering solvent composition-dependent Henry's, nonlinearity, mass-transfer, and diffusion coefficients. (2) A convection−diffusion equation is considered for the evolution of solvent composition. (3) For the first time, different functional relations are introduced and analyzed for quantifying the effect of varying solvent composition on the model parameters. (4) A high-resolution finite-volume scheme (HR-FVS) of Koren[30,31] is extended and applied to solve the model equations. (5) Several case studies are conducted to analyze the influence of solvent strength variation on the elution behavior of concentration profiles. (6) The effects of model parameters are systematically analyzed on the process performance, such as the effects of starting and ending times of the gradient, solvent strength parameter, positive and negative gradients, different gradient models, and nonlinearity coefficients. (7) Determination of numerical moments with

https://doi.org/10.1021/acsomega.4c02444
ACS Omega 2024, 9, 20601−20615

respect to the initial and final gradient times. (8) In order to comprehend the process and forecast the ideal gradient start and end times to attain maximum productivity, evaluation criteria are implemented. (9) The results obtained are useful tools for the practitioners and will provide them basic clues to optimize the operating conditions of their experimental setups and to further upgrade them.

The structure of this article is outlined as follows. Section 2 provides a concise introduction to the one-dimensional LKM. In Section 3, various gradient models are elucidated. Section 4 provides the derivation of the finite-volume method to approximate the model equations, with a specific focus on the HR-FVS of Koren.[30,31] Section 5 introduces the process specification criteria for obtaining the maximum productivity. Section 6 presents case studies and outlines the impacts associated with different model parameters. Concluding remarks and a summary of the findings are provided in Section 7.

2. NONLINEAR LKM OF CHROMATOGRAPHY

The following LKM of gradient elution chromatography is a simplified theoretical framework used to describe and analyze the transport of solute molecules in a column during gradient elution. It is a transport-dispersive model that utilizes a first-order kinetic equation for describing the nonequilibrium effects and its model parameters are functions of varying solvent volume fraction. The mobile-phase mass balance equations for a multicomponent mixture are expressed as

$$\frac{\partial c_i}{\partial t} + u\frac{\partial c_i}{\partial z} = \frac{\partial}{\partial z}\left(D_{z,i}(\varphi)\frac{\partial c_i}{\partial z}\right) - FK_{L,i}(\varphi)(q_i^* - q_i), \quad i = 1, 2..., N_c \tag{1}$$

while the mass balance equations within the solid phase are formulated using kinetic equations of the form

$$\frac{\partial q_i}{\partial t} = K_{L,i}(\varphi)(q_i^* - q_i), \qquad i = 1, 2..., N_c \tag{2}$$

In these equations, the concentration of the ith component of the solute in the fluid's bulk is symbolized by c_i, F is the phase ratio which can be written as $F = \left(\frac{1-\epsilon}{\epsilon}\right)$, ϵ is the external porosity, the symbol $K_{L,i}$ denotes the coefficient that represents the rate of external mass transfer, and the symbol N_c signifies the count of components in the sample mixture. Furthermore, t represents the time, z is the axial coordinate, u is the interstitial velocity, axial dispersion is represented by $D_{z,i}$, and φ is the volume fraction of modifying nonretained solvent, while q_i and q_i^* are nonequilibrium and equilibrium solid-phase concentrations. The initial condition can have a significant effect on the separation process. The initial state of a chromatographic system refers to its condition at the commencement of the separation procedure. For a regenerated column, the initial conditions for concentrations in the liquid and solid phases are specified as follows:

$$c_i(z, 0) = 0, \qquad q_i(z, 0) = 0 \tag{3}$$

Boundary conditions play a crucial role in chromatographic modeling as they establish the physical limitations and constraints of the system. The selection of boundary conditions can significantly impact the predicted retention time, peak shapes, and separation efficiency of the chromatographic column. The boundary conditions at the entrance and outlet of the column are expressed as

$$\frac{D_{z,i}}{u}\frac{\partial c_i(0, t)}{\partial z} + c_i(0, t) = \begin{cases} c_{i,\mathrm{inj}} & 0 \le t \le t_{\mathrm{inj}} \\ 0 & t \ge t_{inj} \end{cases}, \quad \frac{\partial c_i(L, t)}{\partial t} = 0 \tag{4}$$

where L denotes the length of the column.

The following convection−diffusion equation is used for describing variations in modifier concentration

$$\frac{\partial \varphi}{\partial t} + u\frac{\partial \varphi}{\partial z} = \frac{\partial}{\partial z}\left(D_{z,i}(\varphi)\frac{\partial \varphi}{\partial z}\right) \tag{5}$$

For this equation, the initial and boundary conditions are expressed as

$$\varphi(z, 0) = \varphi_0, \qquad 0 \le z \le L \tag{6}$$

$$\varphi(0, t) = \begin{cases} \varphi_0 & \text{if } t < t_s \\ \Phi(t - t_s) & \text{if } t_s \le t \le t_e \\ \varphi_e & \text{if } t \ge t_e \end{cases} \tag{7}$$

In the above equations, the symbols t_s and t_e denote the commencement and termination times of the gradient profile, respectively. Moreover, φ_0 signifies the initial concentration of the solvent, while function Φ denotes the gradient profile programmed into the pump. The concentration of solvent at the end time, t_e, of the gradient is represented by φ_e and is sustained subsequently.

The variation in composition of the mobile phase is known at the inlet of the chromatography column. For a linear gradient, the concentration of the modifier at a given position z in the column is contingent upon both time and the slope of gradient, as defined by

$$\Phi(t) = \varphi_0 + \beta(t - t_s) \tag{8}$$

where $\beta = \frac{\varphi_e - \varphi_0}{t_e - t_s}$ is the slope of the gradient.

The stationary- and mobile-phase concentrations are related to each other through the following Langmuir isotherm

$$q_i^*(c_i, \varphi) = \frac{K_{Hi}(\varphi)c_i}{1 + \sum_{j=1}^{Nc} b_j(\varphi)c_j}, \qquad i = 1, 2, ..., N_c \tag{9}$$

In the aforementioned context, $K_{H,i}$ represents the Henry constant for the ith component, while b_j quantifies the degree of nonlinearity in the isotherm pertaining to the ith component of the mixture. Both parameters are dependent on the composition of the mobile phase.

3. GRADIENT MODELS

Gradient models are essential for optimizing and scaling up chromatographic separations, particularly in industries in which purity and separation efficacy are of the utmost importance. In this study, several gradient models are considered to describe the influence of the solvent composition variation on the movement and distribution of solutes during gradient elution:

https://doi.org/10.1021/acsomega.4c02444
ACS Omega 2024, 9, 20601−20615

3.1. LSS Model. This model describes a linear dependence of the logarithmic model parameters on the solvent volume fraction. Thus, the functional relationships are expressed as

$$K_{H,i}(\varphi) = k_{H,i}^{\mathrm{ref}}\, \mathrm{e}^{-(\alpha\varphi)}, \qquad b_j(\varphi) = b_j^{\mathrm{ref}}\, \mathrm{e}^{-(\alpha\varphi)} \tag{10}$$

$$K_{L,i}(\varphi) = k_{L,i}^{\mathrm{ref}}\, \mathrm{e}^{-(\gamma\varphi)}, \qquad D_{z,i}(\varphi) = D_{z,i}^{\mathrm{ref}}\, \mathrm{e}^{-(\gamma\varphi)} \tag{11}$$

3.2. Quadratic Strength Model. In the quadratic strength model, relationships between model parameters and the solvent volume fraction are expressed in the form of quadratic functions, allowing for a more detailed representation of the gradient elution behavior. Mathematically, such relationships are depicted as

$$K_{H,i}(\varphi) = k_{H,i}^{\mathrm{ref}}\, \mathrm{e}^{-(\alpha_1\varphi+\alpha_2\varphi^2)}, \quad b_j(\varphi) = b_j^{\mathrm{ref}}\, \mathrm{e}^{-(\alpha_1\varphi+\alpha_2\varphi^2)} \tag{12}$$

$$K_{L,i}(\varphi) = k_{L,i}^{\mathrm{ref}}\, \mathrm{e}^{-(\gamma_1\varphi+\gamma_2\varphi^2)}, \quad D_{z,i}(\varphi) = D_{z,i}^{\mathrm{ref}}\, \mathrm{e}^{-(\gamma_1\varphi+\gamma_2\varphi^2)} \tag{13}$$

3.3. Neue−Kuss Model. The Neue and Kuss model is a nonlinear solvent strength model of gradient elution chromatography. In this case, the functional relationships are given as

$$K_{H,i}(\varphi) = k_{H,i}^{\mathrm{ref}}(1+\alpha_2\varphi)^2\, \mathrm{e}^{-\alpha_1\varphi/1+\alpha_2\varphi}, \quad b_j(\varphi) = b_j^{\mathrm{ref}}(1+\alpha_2\varphi)^2\, \mathrm{e}^{-\alpha_1\varphi/1+\alpha_2\varphi} \tag{14}$$

$$K_{L,i}(\varphi) = k_{L,i}^{\mathrm{ref}}(1+\gamma_2\varphi)^2\, \mathrm{e}^{-\gamma_1\varphi/1+\gamma_2\varphi}, \quad D_{z,i}(\varphi) = D_{z,i}^{\mathrm{ref}}(1+\gamma_2\varphi)^2\, \mathrm{e}^{-\gamma_1\varphi/1+\gamma_2\varphi} \tag{15}$$

3.4. Power-Law Model. This model provides the following functional relationships between model parameters and solvent volume fraction

$$K_{H,i}(\varphi) = k_{H,i}^{\mathrm{ref}}\varphi^{-n}, \qquad b_j(\varphi) = b_j^{\mathrm{ref}}\varphi^{-n} \tag{16}$$

$$K_{L,i}(\varphi) = k_{L,i}^{\mathrm{ref}}\varphi^{-n}, \qquad D_{z,i} = D_{z,i}^{\mathrm{ref}}\varphi^{-n} \tag{17}$$

The reference values for Henry, mass-transfer, nonlinearity, and axial dispersion coefficients for the specific component are denoted by letters $k_{H,i}^{\mathrm{ref}}$, $k_{L,i}^{\mathrm{ref}}$, b_j^{ref}, and $D_{z,i}^{\mathrm{ref}}$, respectively. The volume fraction of modifying nonretained solvent is represented by φ, and the solvent-specific strength parameters are dented by α_1, α_2, γ_1, and γ_2.

4. HR-FVS OF KOREN

The Koren finite-volume scheme[30] is a powerful and versatile numerical method for solving convection−diffusion equations, and it is known for its accuracy, robustness, and ease of implementation. For numerical approximation of the nonlinear LKM of gradient elution chromatography presented in this work, we have extended the HR-FVS of Koren.

4.1. Framework of the Scheme. The basic steps are as follows:

(1) A finite number of grids are created along the axial coordinate of the column to divide the axial computational domain.

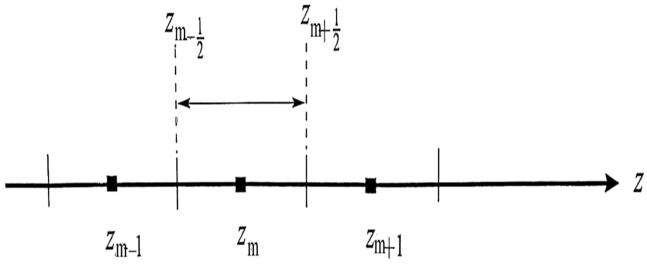

Figure 1. Finite-volume mesh (centered at the cell).

(2) To estimate concentrations in each control volume using the integral conservation law, the domain is first divided into a number of control volumes. Hence, conservation equations are discretized in terms of the axial coordinate.

(3) The main objective of this discretization process is to produce a set of coupled ODEs in terms of the time coordinate.

(4) The resulting ODE system is solved through an ODE solver.

(5) MATLAB software is utilized to implement the algorithm and a built-in RK-45 solver is utilized to solve the resulting ODE system.

4.2. Discretization of PDEs for Mobile-Phase Concentration. As mentioned in the above steps, we start with the discretization of the computational domain before applying the finite-volume scheme to eqs 1−17. Let N be the number of discretization points, $z_{m\mp\frac{1}{2}}$ symbolizes the left and right boundaries of the interval (control volume), Δz stands for the cell width, and z_m denotes the cell centers as shown in Figure 1.

Furthermore, let us assign the following

$$z_{N+\frac{1}{2}} = L, \qquad z_{1/2} = 0, \qquad z_{m+\frac{1}{2}} = m\Delta z \tag{18}$$

and

$$z_m = \frac{z_{m-\frac{1}{2}} + z_{m+\frac{1}{2}}}{2}, \quad \Delta z = z_{m+\frac{1}{2}} - z_{m-\frac{1}{2}} = \frac{L}{N+1} \tag{19}$$

Let $\Omega_m = \left[z_{m-\frac{1}{2}}, z_{m+\frac{1}{2}}\right]$ for $m \geq 1$. The averaged initial data $w_m(0)$ is formulated in each interval as

$$w_m(0) = \frac{1}{\Delta z}\int_{z_{m-\frac{1}{2}}}^{z_{m+\frac{1}{2}}} w(z,0)\,\mathrm{d}z, \quad w \in \{c_i, q_i, q_i^*\}, \qquad m = 1, 2, \ldots, N \tag{20}$$

Integration of eqs 1 and 2 over the interval $\Omega_i = \left[z_{i-\frac{1}{2}} - z_{i+\frac{1}{2}}\right]$ leads to

$$\int_{z_{m-\frac{1}{2}}}^{z_{m+\frac{1}{2}}} \frac{\partial c_i}{\partial t}\,\mathrm{d}z + u\int_{z_{m-\frac{1}{2}}}^{z_{m+\frac{1}{2}}} \frac{\partial c_i}{\partial z}\,\mathrm{d}z = \int_{z_{m-\frac{1}{2}}}^{z_{m+\frac{1}{2}}} \frac{\partial}{\partial z}\left(D_{z,i}(\varphi)\,\frac{\partial c_i}{\partial z}\right)\mathrm{d}z - \int_{z_{m-\frac{1}{2}}}^{z_{m+\frac{1}{2}}} FK_L(\varphi)(q_i^* - q_i)\,\mathrm{d}z, \qquad i = 1, 2 \tag{21}$$

https://doi.org/10.1021/acsomega.4c02444
ACS Omega 2024, 9, 20601−20615

and

$$\int_{z_{m-\frac{1}{2}}}^{z_{m+\frac{1}{2}}} \frac{\partial q_i}{\partial t}\,\mathrm{d}z = \int_{z_{m-\frac{1}{2}}}^{z_{m+\frac{1}{2}}} K_L(\varphi)(q_i^* - q_i)\,\mathrm{d}z \tag{22}$$

For each Ω_m, the average values of a conservative variable $w(t)$ are given as

$$w_m := w_m(t) = \frac{1}{\Delta z}\int_{z_{m-\frac{1}{2}}}^{z_{m+\frac{1}{2}}} w(t, z)\,\mathrm{d}z,$$
$$w \in \{c_i, q_i, q_i^*\}, \qquad m = 1, 2, \ldots, N \tag{23}$$

Now, for $m = 1, 2, \cdots\cdots, N$, we obtain a semidiscrete scheme of the form

$$\frac{\mathrm{d}c_{i,m}}{\mathrm{d}t} = -\frac{uc_i}{\Delta z}\Bigg|_{z_{m-\frac{1}{2}}}^{z_{m+\frac{1}{2}}} + \left[\frac{D_{z,i}(\varphi_m(t))}{\Delta z}\frac{\partial c_i}{\partial z}\right]\Bigg|_{z_{m-\frac{1}{2}}}^{z_{m+\frac{1}{2}}} - FK_L(\varphi_m(t))(q_{i,m}^* - q_{i,m}), \qquad i = 1, 2 \tag{24}$$

or

$$\frac{\mathrm{d}c_{i,m}}{\mathrm{d}t} = -u\frac{c_{i,m+\frac{1}{2}} - c_{i,m-\frac{1}{2}}}{\Delta z} + \frac{1}{\Delta z}\left[\left(D_{z,i}(\varphi(t))\frac{\partial c_i}{\partial z}\right)_{i,m+\frac{1}{2}} - \left(D_{z,i}(\varphi(t))\frac{\partial c_i}{\partial z}\right)_{i,m-\frac{1}{2}}\right] - FK_L(\varphi_m(t))(q_{i,m}^* - q_{i,m}), \qquad i = 1, 2 \tag{25}$$

and

$$\frac{\mathrm{d}q_{i,m}}{\mathrm{d}t} = K_L(\varphi_m(t))(q_{i,m}^* - q_{i,m}), \qquad i = 1, 2 \tag{26}$$

The terms in eq 25 can be approximated as

$$\left[\frac{\partial c_i}{\partial z}\right]_{m\pm\frac{1}{2}} = \frac{c_{i,m\pm1} - c_{i,m}}{\Delta z} \tag{27}$$

and

$$[D_{z,i}(\varphi(t))]_{m\pm\frac{1}{2}} = \left[\frac{(D_{z,i})_m + (D_{z,i})_{m\pm1}}{2}\right] \tag{28}$$

4.3. Discretization of PDE for Modifier Concentration. Integrating eq 5 over the interval $\Omega_m = \left[z_{m-\frac{1}{2}}, z_{m+\frac{1}{2}}\right]$, we obtain

$$\int_{z_{m-\frac{1}{2}}}^{z_{m+\frac{1}{2}}} \frac{\partial \varphi}{\partial t}\,\mathrm{d}z + u\int_{z_{m-\frac{1}{2}}}^{z_{m+\frac{1}{2}}} \frac{\partial \varphi}{\partial z}\,\mathrm{d}z = \int_{z_{m-\frac{1}{2}}}^{z_{m+\frac{1}{2}}} \frac{\partial}{\partial z}\left(D_z(\varphi)\frac{\partial \varphi}{\partial z}\right)\mathrm{d}z \tag{29}$$

By using eq 23, we obtain a semidiscrete scheme as follows

$$\frac{\mathrm{d}\varphi_m}{\mathrm{d}t} = -\frac{u\phi}{\Delta z}\Bigg|_{z_{m-\frac{1}{2}}}^{z_{m+\frac{1}{2}}} + \left[\frac{D_z(\varphi(t))}{\Delta z}\frac{\partial \varphi}{\partial z}\right]\Bigg|_{z_{m-\frac{1}{2}}}^{z_{m+\frac{1}{2}}} \tag{30}$$

or

$$\frac{\mathrm{d}\varphi_m}{\mathrm{d}t} = -u\frac{\varphi_{m+\frac{1}{2}} - \varphi_{m-\frac{1}{2}}}{\Delta z} + \frac{1}{\Delta z}\left[\left(D_z(\varphi(t))\frac{\partial \varphi}{\partial z}\right)_{m+\frac{1}{2}} - \left(D_z(\varphi(t))\frac{\partial \varphi}{\partial z}\right)_{m-\frac{1}{2}}\right] \tag{31}$$

The terms in eq 31 can be approximated as

$$\left[\frac{\partial \varphi}{\partial z}\right]_{m\pm\frac{1}{2}} = \pm\frac{\varphi_{m\pm1} - \phi_m}{\Delta z} \tag{32}$$

and

$$[D_z(\varphi(t))]_{m\pm\frac{1}{2}} = \left[\frac{(D_z)_m + (D_z)_{m\pm1}}{2}\right] \tag{33}$$

There are different techniques in the literature to approximate cell-interface fluxes in eqs 25 and 31. Consider the inequality $u \geq 0$ and using the Koren scheme,[30,31] we obtain the following approximations of $c_{i,m\pm\frac{1}{2}}$ and $\phi_{m\pm\frac{1}{2}}$.

4.4. First-Order Approximation. The cell-interface fluxes are approximated as

$$c_{i,m+\frac{1}{2}} = c_{i,m}, \qquad \text{and} \qquad c_{i,m-\frac{1}{2}} = c_{i,m-1} \tag{34}$$

$$\varphi_{m+\frac{1}{2}} = \phi_m, \qquad \text{and} \qquad \varphi_{m-\frac{1}{2}} = \phi_{m-1} \tag{35}$$

A scheme accurate to the first order in the axial direction is obtained through this approximation.

However, at least second-order approximations of the cell-interface fluxes are required for capturing sharp fronts in the solutions. Thus, we need the following approximation.

4.5. Koren Scheme. Koren[30] is applied here to obtain better approximations of the cell-interface fluxes

$$c_{i,m+\frac{1}{2}} = c_{i,m} + \frac{1}{2}\Psi\left[r_{i,m+\frac{1}{2}}\right][c_{i,m} - c_{i-1,m}] \tag{36}$$

$$\varphi_{m+\frac{1}{2}} = \varphi_m + \frac{1}{2}\Theta\left[s_{m+\frac{1}{2}}\right][\varphi_m - \varphi_{m-1}] \tag{37}$$

where $r_{m+\frac{1}{2}}$ and $s_{m+\frac{1}{2}}$ are the ratios of gradients for consecutive fluxes

$$r_{m+\frac{1}{2}} = \frac{c_{i,m+1} - c_{i,m} + \zeta}{c_{i,m} - c_{i,m-1} + \zeta} \tag{38}$$

$$s_{m+\frac{1}{2}} = \frac{\varphi_{m+1} - \varphi_m + \zeta}{\varphi_m - \varphi_{m-1} + \zeta} \tag{39}$$

Here, in the denominator of eqs 38 and 39, we may get zero value. Thus, to avoid this, we chose $\zeta \approx 10^{-10}$. Furthermore, in eqs 36 and 37, Ψ and Θ are the limiting functions as expressed below

$$\Psi\left[r_{m+\frac{1}{2}}\right] = \max\left[0, \min\left[2r_{m+\frac{1}{2}}, \min\left[\frac{1}{3} + \frac{2}{3}r_{i+\frac{1}{2}}, 2\right]\right]\right] \tag{40}$$

$$\Theta\left[s_{m+\frac{1}{2}}\right] = \max\left[0, \min\left[2s_{m+\frac{1}{2}}, \min\left[\frac{1}{3} + \frac{2}{3}s_{i+\frac{1}{2}}, 2\right]\right]\right] \tag{41}$$

https://doi.org/10.1021/acsomega.4c02444
ACS Omega 2024, 9, 20601−20615

Table 1. Reference Parameters Used for the Simulation Process

parameter name	experimental values
column length	$L = 10.0$ [cm]
porosity	$\epsilon = 0.4$
velocity (interstitial)	$u = 0.6$ [cm/min]
reference axial dispersion coefficient	$D_z^{\mathrm{ref}} = 0.0002$ [cm^2/min]
reference Henry constant component I	$k_{H,1}^{\mathrm{ref}} = 1.5$
reference Henry constant component II	$k_{H,2}^{\mathrm{ref}} = 4.0$
reference nonlinearity coefficient component I	$b_1^{\mathrm{ref}} = 1.0$
reference nonlinearity coefficient component II	$b_2^{\mathrm{ref}} = 1.5$
solvent strength parameter	$\alpha = 0.9$
solvent strength parameter (QSS, Neue, and power law)	$\alpha_1 = 0.9$
solvent strength parameter(QSS, Neue, and power law)	$\alpha_2 = 0.8$
mass-transfer coefficient	$k_L^{\mathrm{ref}} = 10$ [min^{-1}]
initial concentration	$\varphi_0 = 0.1$
final concentration	$\varphi_e = 0.95$
gradient start time	$t_s = 5$ [min]
gradient end time	$t_e = 80$ [min]
order of the power-law model	$n = 1$

Here, the above eqs 36 and 37 give a second-order accurate scheme. The built-in RK-45 in MATLAB is used for solving the resulting ODE system in eqs 25, 26, and 31.

4.6. Scheme Strategy at Boundaries. The approximations outlined in eqs 36 and 37 are not suitable for the boundary intervals. Let us assume the left boundary within the flow boundary condition. To avoid this issue, the first-order approximation of 36 and 37 can be utilized at the cell interfaces $z_{3/2}$ and $z_{N+\frac{1}{2}}$. The fluxes at additional cell boundaries can be estimated through the application of the high-resolution finite-volume method discussed above.

5. SPECIFICATIONS FOR PROCESS PERFORMANCE

Process specification criteria play a pivotal role in ensuring the maximum productivity within various industries. The optimization of gradient elution chromatography necessitates the establishment of appropriate performance criteria. In this context, we introduce a performance criterion designed to improve product quality.[32,33] We examine a binary mixture $N_c = 2$, where component 1 exhibits lower retention compared to component 2, denoted as $k_{H,1}^{\mathrm{ref}} < k_{H,2}^{\mathrm{ref}}$. Let us assume that t_1 represents the time during which the fraction of the first component surpasses a specific threshold, that is, $c_1 \geq \tilde{\epsilon} c_{1,\mathrm{inj}}$, with $\tilde{\epsilon} = 10^{-5}$. Additionally, let t_2 denote the duration within which the fraction of the second component falls below a designated threshold, namely, $c_2 \leq \tilde{\epsilon} c_{2,\mathrm{inj}}$. Key performance metrics in this study are cycle time, purity, productivity, and yield. Here, cycle time, productivity, and yield serve as performance measures, while purity functions as a constraint.

5.1. Cycle Time. The cycle time, denoted as t_{cyc}, is characterized as the time between two consecutive injections.

$$t_{\mathrm{cyc}} = t_2 - t_1 \tag{42}$$

5.2. Purity. The instant when the fractionation process for component 1 terminates is widely referred to as the "cut time." We utilize the subsequent expression in our computations to determine the cut time, represented as t_{cut} for component 1

$$\mathrm{Pur} = \frac{\int_{t_1}^{t_{\mathrm{cut}}} c_1(x=1,t)\,\mathrm{d}t}{\int_{t_1}^{t_{\mathrm{cut}}} [c_1(x=1,t) + c_2(x=1,t)\,\mathrm{d}t]\,\mathrm{d}t} \tag{43}$$

The designated purity level was established at 99% as determined by the peak area.

5.3. Productivity. The term "reduced productivity" Y^{Pr} represents the desired quantity of the compound produced within a specific time cycle. For component 1, it is evaluated as

$$Y^{\mathrm{Pr}} = \frac{\int_{t_1}^{t_{\mathrm{cut}}} c_1(x=1,t)\,\mathrm{d}t}{t^{\mathrm{cyc}}} \tag{44}$$

5.4. Yield. The recovery yield is calculated as the proportion of the desired component in the purified fraction relative to the amount initially introduced at the column's inlet. Specifically, for the first eluting component, the recovery yield is characterized as

$$Y = \frac{\int_{t_1}^{t_{\mathrm{cut}}} c_1(t,x=1)\,\mathrm{d}t}{\int_{t_1}^{t_2} c_1(t,x=1)\,\mathrm{d}t} \tag{45}$$

6. CASE-BY-CASE ASSESSMENTS OF PARAMETRIC EFFECTS

In this section, we explore the behavior of gradient elution chromatography under varying operating conditions and for different relationships between model parameters and solvent composition. Moreover, we conduct an in-depth analysis of the efficiency and accuracy of the proposed numerical algorithm. In all test problems, the solute concentrations (c) and the modulator concentration (ϕ) are plotted at the outlet of the column $(z = L)$. Thus, for current nonretained solvent composition, the gradient start time at the column outlet is $t_s + L/u$ and the end time is $t_e + L/u$ as can be observed in the plots. Here, L/u symbolizes the time needed for a nonretained solvent composition to reach the other end

https://doi.org/10.1021/acsomega.4c02444
ACS Omega 2024, 9, 20601−20615

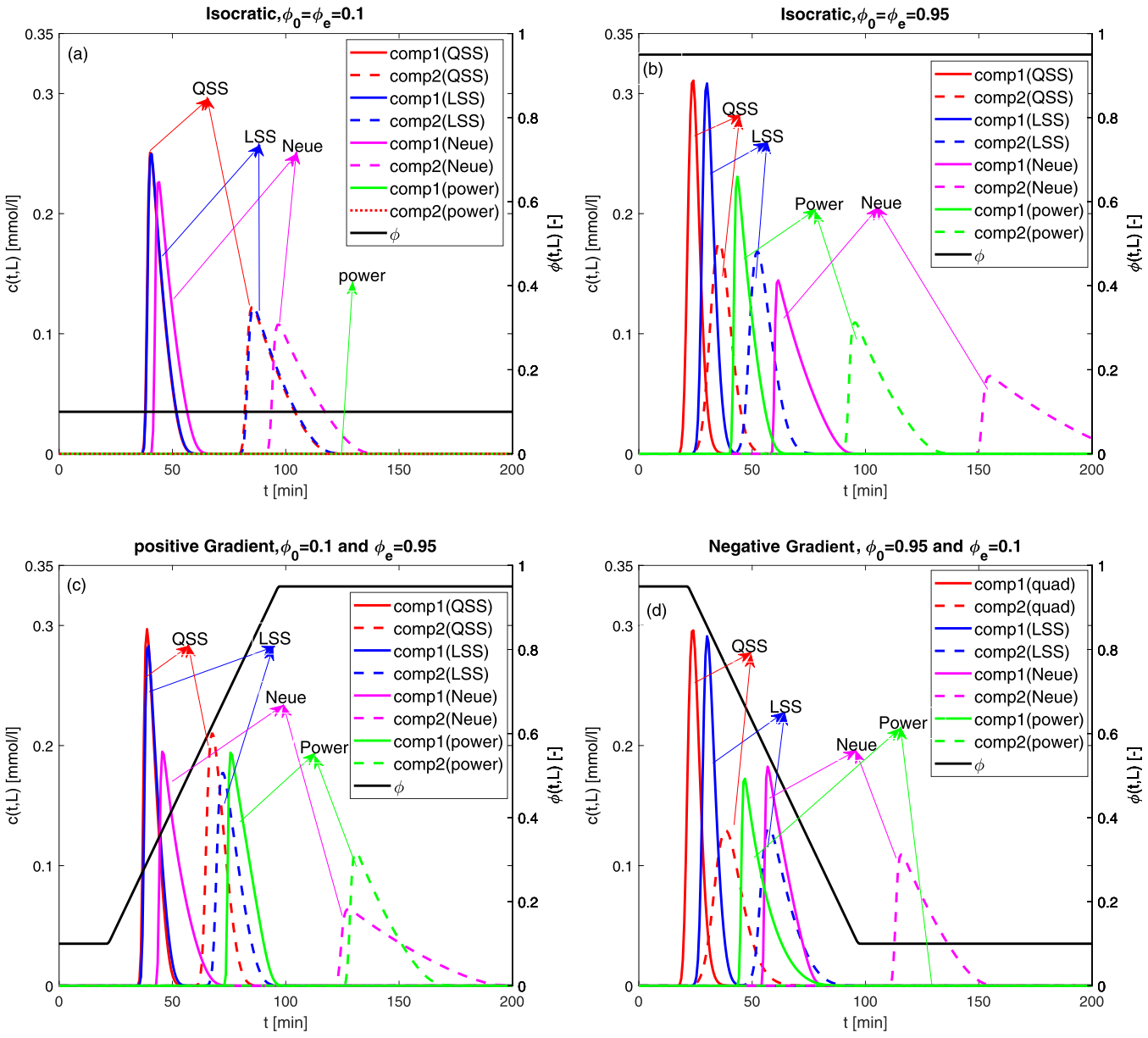

Figure 2. Comparison of isocratic [top plots, figure (a,b)] and gradient elution [bottom plots, figure (c,d)].

of the column. Table 1 provides a list of reference parameters for all case studies that have been utilized. The values of these parameters are selected from the available ranges commonly utilized in liquid chromatography operations.

6.1. Comparison of Isocratic and Gradient Elution. A comparison of different types of gradient models is presented in Figure 2, for both isocratic and gradient elution. In Figure 2a for the value of $\phi = \phi_0 = 0.1$ (low concentration of the mobile phase), the QSS and LSS models overlap each other and provide better separation and efficiency of the column. It is worth emphasizing that at such a low concentration of the mobile phase, the power-law model proves entirely ineffective and does not yield the desired results (namely, baseline separation) for either of the components. In Figure 2b, considering $\phi = \phi_e = 0.95$ (i.e., high concentration of the mobile phase), it can be observed that the peaks of the QSS and LSS exhibit narrower profiles and shorter retention times. In this scenario, the power-law model produces superior results compared to the Neue−Kuss model. In Figure 2c,d, representing the positive and negative gradients, it becomes evident that the QSS and LSS models outperform the others in terms of separation and efficiency. Overall, the QSS model gives the best result as compared to other models.

6.2. Effect of Reference Axial Dispersion Coefficient. Figure 3 shows the influence of the reference axial dispersion coefficient D_z^{ref} on various gradient models. In Figure 3a, it is observed that the eluted profile peaks generated by all gradient models exhibit diffusivity and increased width when the value of D_z^{ref} is set to 0.2 cm^2 min^{-1}, leading to extended retention times. In Figure 3b, the concentration profiles associated with all gradient models exhibit reduced broadening, as the value of D_z^{ref} decreases to 0.002 cm^2 min^{-1}. In summary, it becomes apparent that variations in the mobile phase-dependent axial dispersion coefficient have substantial implications for separation and peak morphology.

6.3. Effect of Gradient Start Time. Figure 4 illustrates the influence of gradient start time t_s on nonlinear elution profiles involving two components. When we increment the

https://doi.org/10.1021/acsomega.4c02444
ACS Omega 2024, 9, 20601−20615

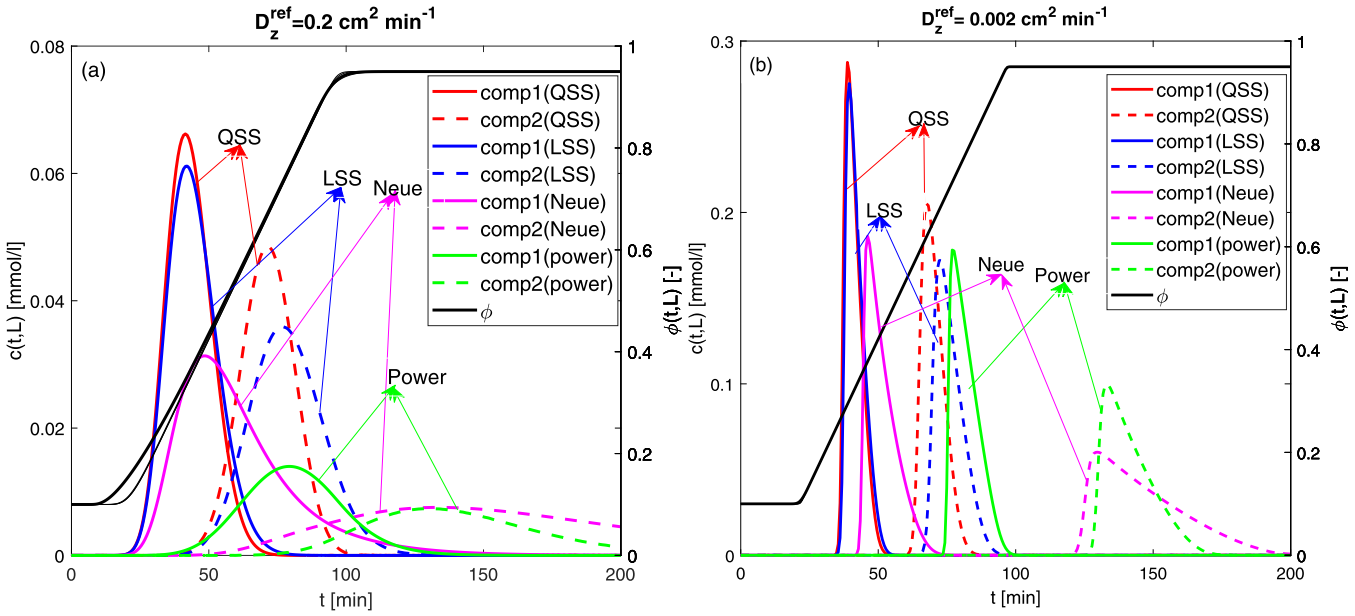

Figure 3. Impact of variations in reference axial dispersion coefficient values on the eluted profiles for all gradient models.

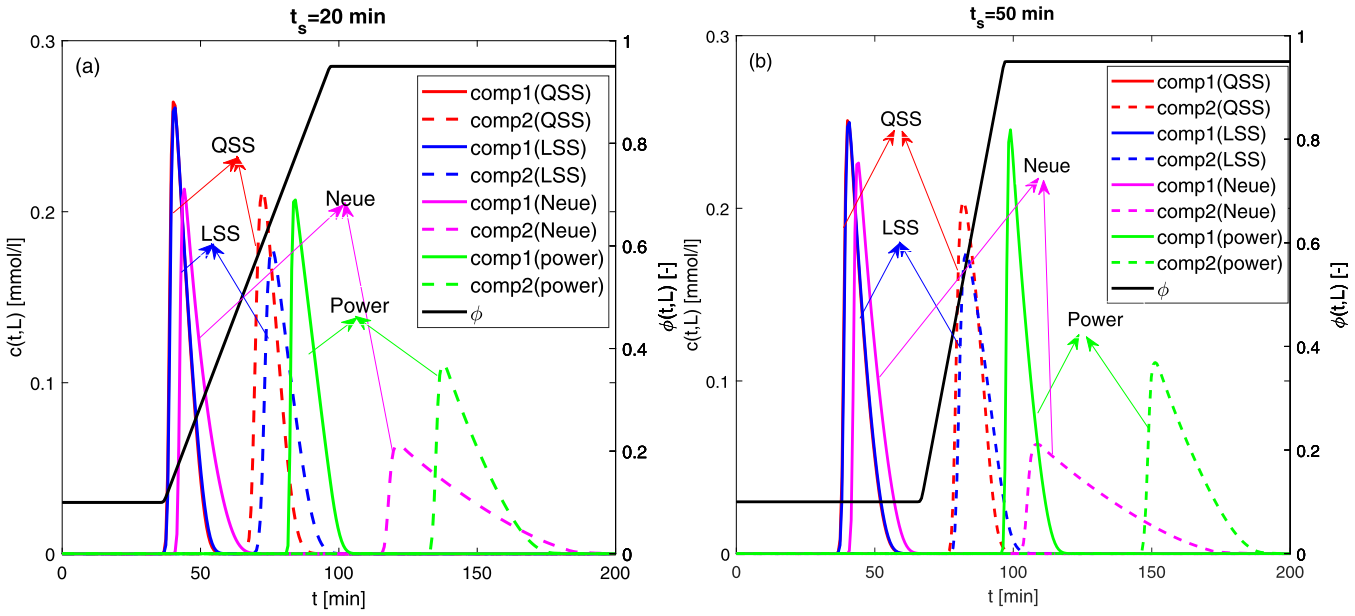

Figure 4. Impacts resulting from the alteration of the initial time for all gradient models.

value of t_s from 20 to 50 min, the LSS, QSS, and Neue−Kuss models demonstrate enhanced separation, characterized by the overlapping of elution peaks. Conversely, the power-law model does not exhibit a significant effect with an increase in the gradient starting time. In conclusion, a gradient starting time of t_s = 20 min represents the optimal selection for the gradient elution process.

6.4. Effect of Gradient End Time. Figure 5 illustrates the influence of gradient end time, denoted by t_e, on nonlinear elution profiles. Versatile behavior can be seen in Figure 5a,b. On increasing t_e = 20 min to t_e = 65 min, the peak heights reduce for both the QSS and LSS models. Peaks generated using Neue−Kuss models show a decrease in retention time. Moreover, employing shallower gradients in the power-law model leads to a deceleration of the chromatograms. Each gradient model yields better resolution of peaks and, thus, improved component separation and column efficiency.

6.5. Effect of Reference Nonlinearity Coefficient. Figure 6 demonstrates the impact of reference nonlinearity coefficients, b_j^{ref}, j = 1, 2, on the nonlinear two-component elution profiles. In Figure 6a, it is seen that for b_j^{ref} = 0, j = 1, 2, all gradient models exhibit narrow peaks characterized by a Gaussian shape. However, it is noteworthy that the peaks presented by the power-law model are narrower in comparison with those of the other models. A narrow profile enhances the efficiency, purity, and column efficiency. As b_j^{ref} increases incrementally, the peaks generated by all gradient models become asymmetrical and broaden, ensuring that the considered gradient elution process yields accurate, reproducible, and high-quality results. Notably, the Neue−Kuss

https://doi.org/10.1021/acsomega.4c02444
ACS Omega 2024, 9, 20601−20615

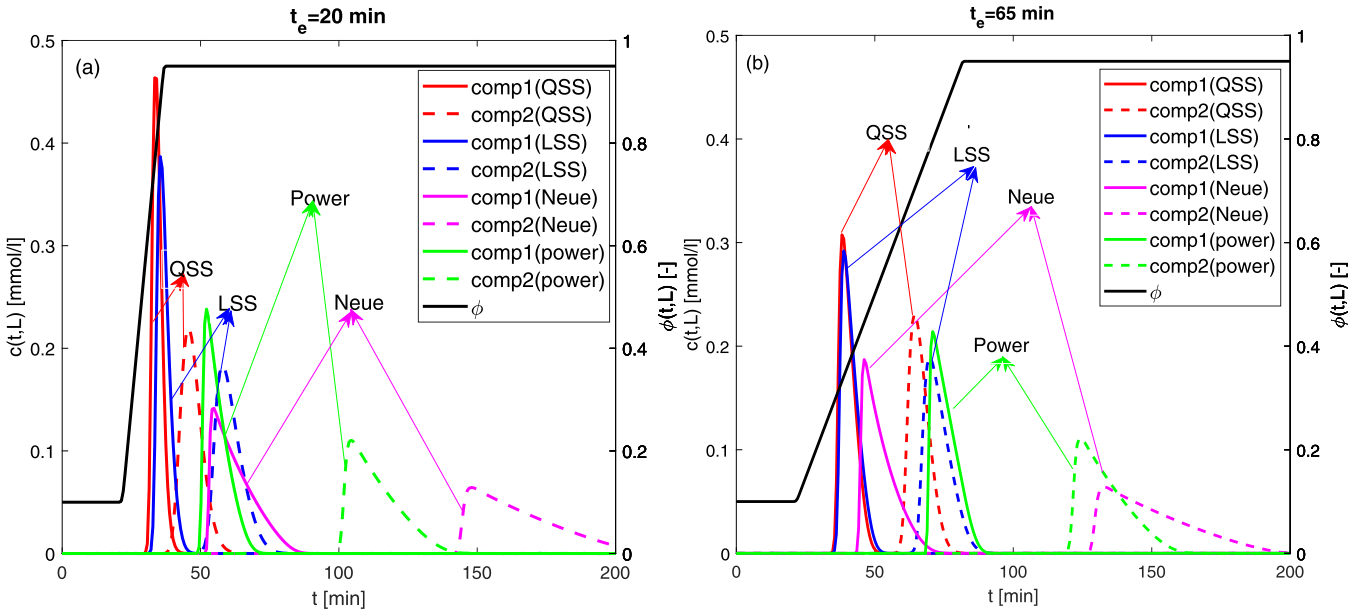

Figure 5. Effects generated by varying the ending time of all gradient models.

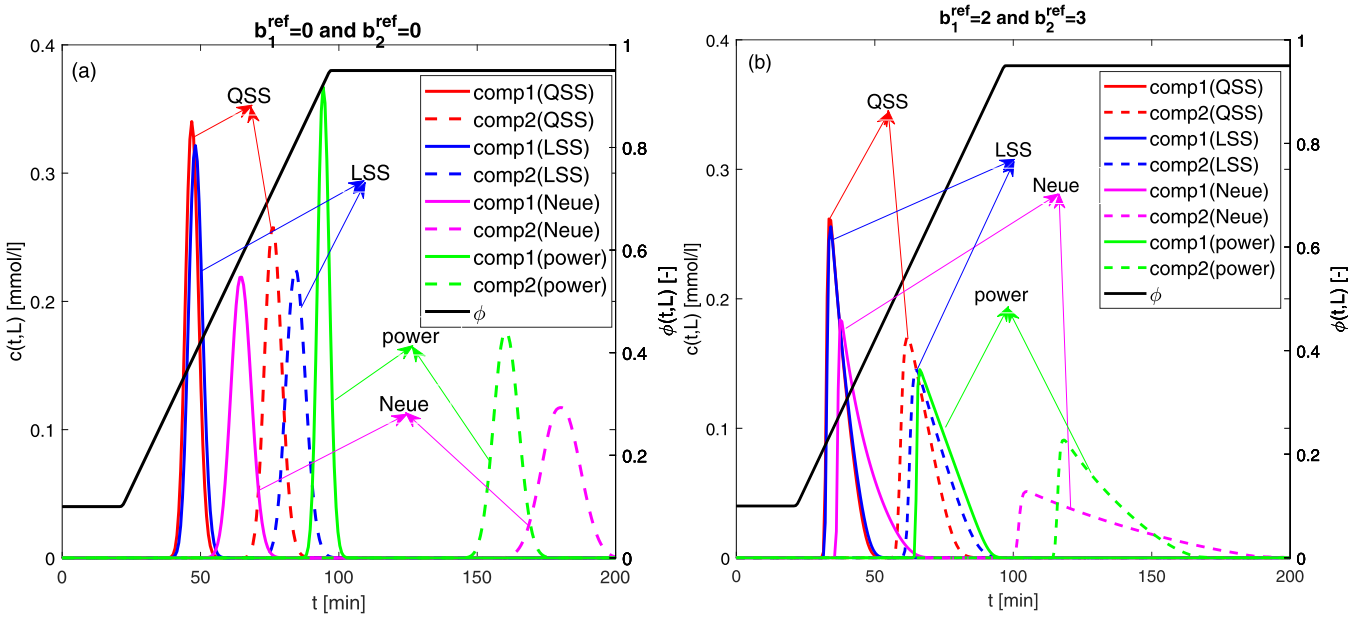

Figure 6. Impact of reference nonlinearity coefficients b_j^{ref}, j = 1, 2 on the elution profiles produced by all models.

model and the power-law model exhibit a significant reduction in retention time under these conditions.

6.6. Effect of Reference Henry Constant. Figure 7 represents the results of varying the reference Henry constant $k_{H,i}^{\mathrm{ref}}$, i = 1, 2 to analyze the partitioning of a solute between the mobile and stationary phases and its effect on the retention time and overall separation efficacy by using different gradient models. A comparison is presented between two distinct sets of $k_{H,i}^{\mathrm{ref}}$, i = 1, 2. The first scenario, denoted as (a), is characterized by $k_{H,1}^{\mathrm{ref}}$ = 1 and $k_{H,2}^{\mathrm{ref}}$ = 2, while the second scenario, marked as (b), involves $k_{H,1}^{\mathrm{ref}}$ = 2 and $k_{H,2}^{\mathrm{ref}}$ = 3. These configurations are chosen for verifying potential implications arising due to different choices of reference constants. All gradient models give narrower peaks with less retention time (in particular, QSS and LSS have better performance) for choice (a). The second scenario with higher Henry's constant indicates a stronger interaction of the analyte with the stationary phase, leading to increased retention time and broadened peaks.

6.7. Effect of Reference Mass-Transfer Coefficient. Figure 8 shows the effect of the reference mass-transfer coefficient $k_{L,i}^{\mathrm{ref}}$ on nonlinear two-component elution profiles. Higher efficiency of the chromatographic column is associated with the optimal mass transfer between the two phases. Figure 8a illustrates the augmentation of peak dispersion, a consequence attributed to the delayed migration of solutes from the mobile phase to the stationary phase, whereas Figure 8b shows that increasing the reference mass-transfer coefficient results in narrow, asymmetrical peaks and no effect on retention time as expected. This is a sign of the equilibrium adsorption within the column, which is controlled

https://doi.org/10.1021/acsomega.4c02444
ACS Omega 2024, 9, 20601−20615

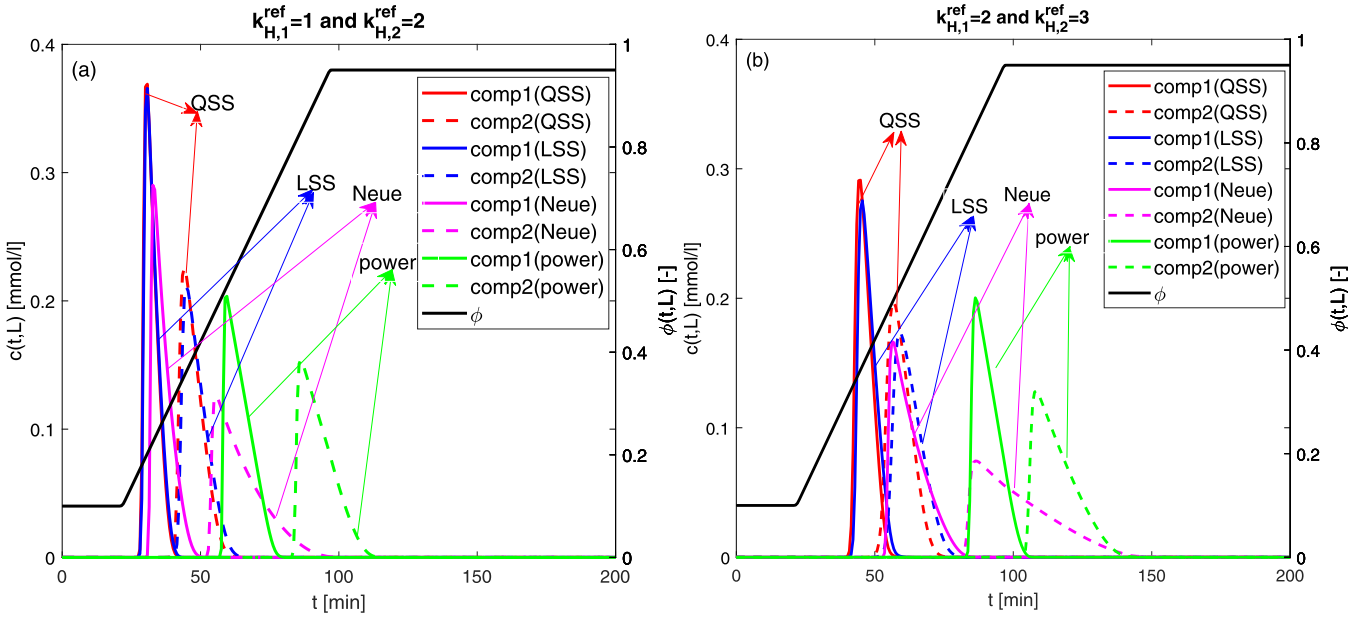

Figure 7. Influence of the reference Henry constant $k^{ref}_{H,i}$, i = 1, 2.

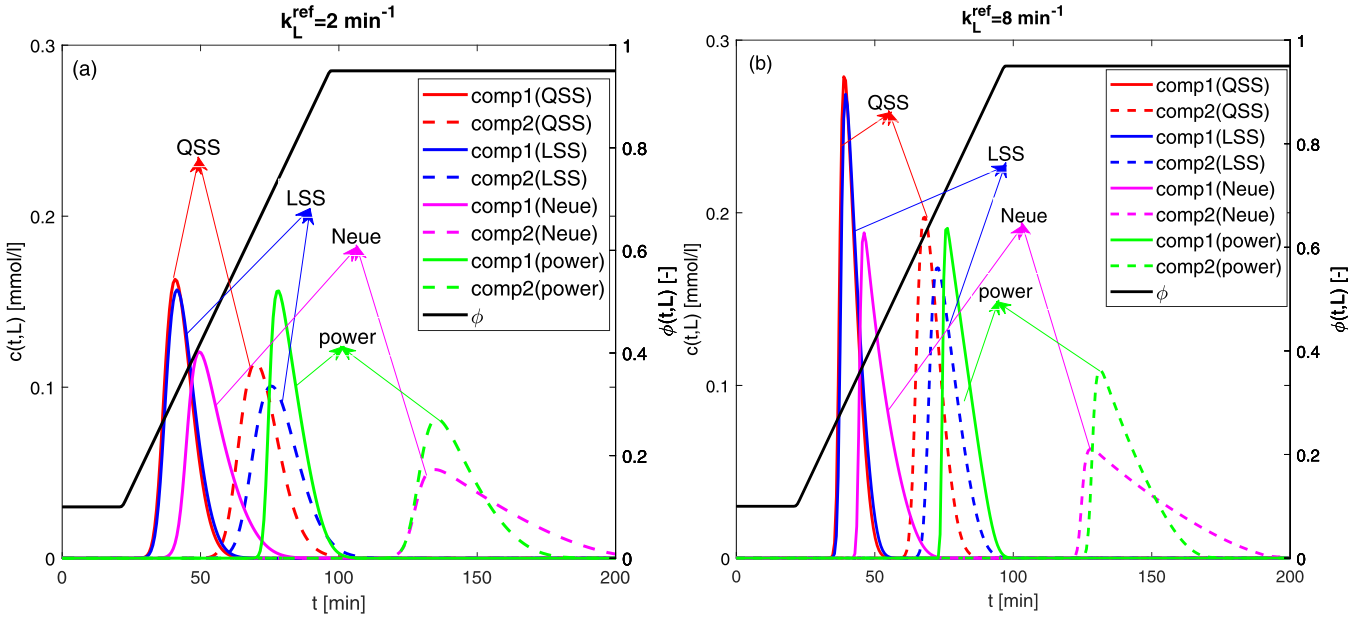

Figure 8. Influence of the mass-transfer coefficient k^{ref}_{L}.

by different gradient models and leading to better separation efficiency of the column.

6.8. Effects of Gradient Time on Moments of Component 1. Figures 9 and 10 illustrate the impact of altering the starting and ending times of the gradients individually for a constant gradient steepness and magnitude on the moments of component 1, considering the LSS model and the reference parameters given in Table 1.

The impact of modulator starting time t_s with a constant ending time of 80 min on the numerical moments is illustrated in Figure 9. Moment plots illustrate that the inclusion of steeper gradients, i.e., delaying the beginning of the gradient, causes the peaks to spread out (peak height lowers) and develop longer tails, while the chromatograms slow down. This pattern will also terminate if the gradients are sufficiently steep, at which point the initial elution strength will control the elution. The inflection point for t_s is depicted to be between t_s = 20 and t_s = 40 min, where a transition region can be seen.

Figure 10 illustrates the impact of gradient ending time (t_e) on the numerical moments, assuming a constant starting time of t_s = 5 min. If t_e = t_s = 5 min, then there is an instantaneous transition to the isocratic state following this brief interval. This is a limiting scenario. As illustrated in Figure 2, this delay results in a marginal reduction in the second and third moments, while a marginal increase in the first moment, in comparison to the entirely isocratic case. By increasing the ending time, which results in the introduction of shallower gradients, the chromatograms are decelerated, and the peaks become more pronounced and symmetrical. This trend, however, ceases when the gradients become so shallow that the initial elution strength governs the elution.

https://doi.org/10.1021/acsomega.4c02444
ACS Omega 2024, 9, 20601−20615

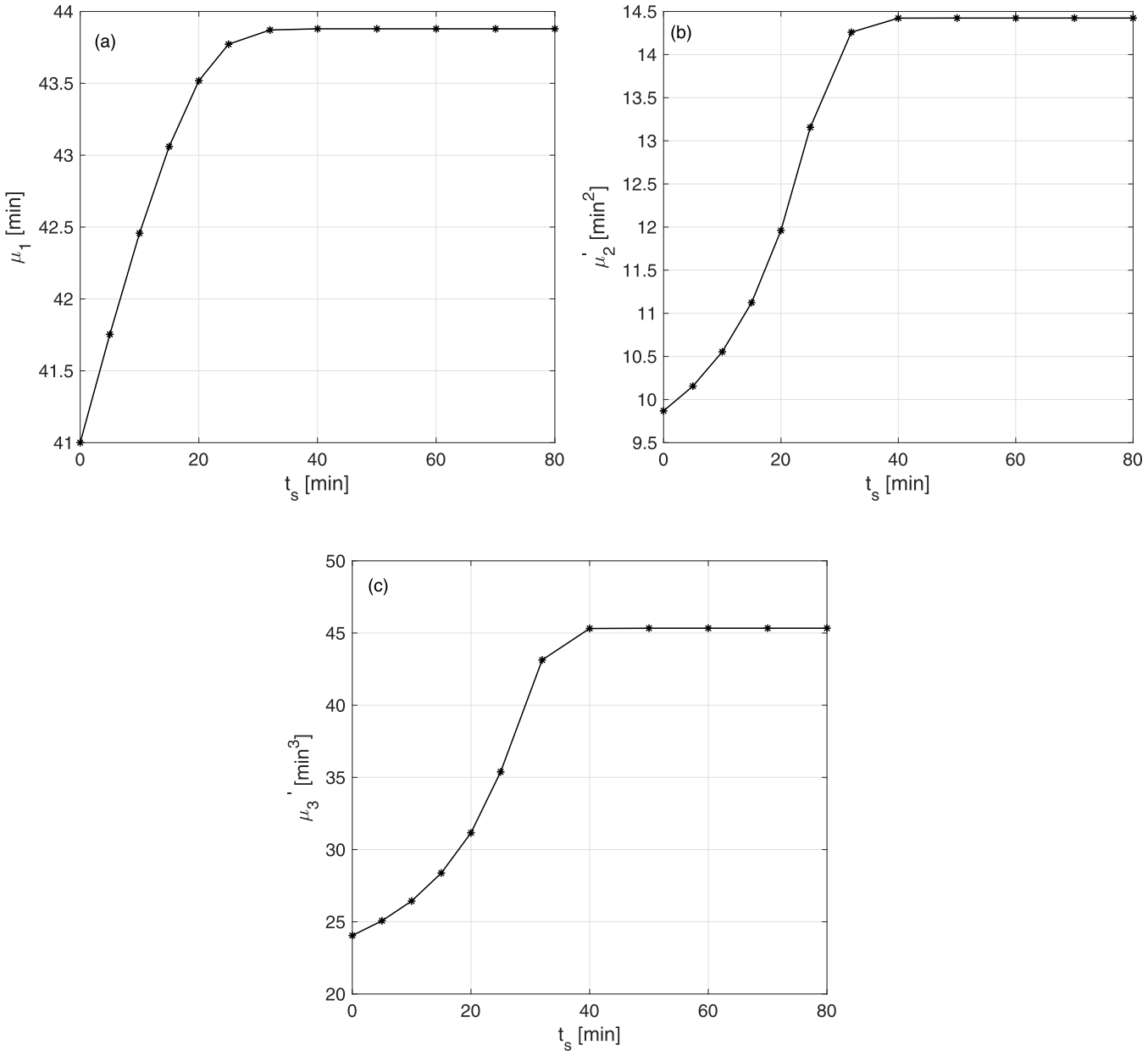

Figure 9. Effects of gradient start time on the moments for component 1 obtained by numerical integration, considering the LSS gradient model and the reference parameters given in Table 1, while t_s was gradually changed.

The turning point in the specific example depicted occurs at approximately t_e = 24 min and is valid just for the specific parameters considered.

6.9. Evaluation of Process Performance. The process performance in the case of the two-component mixture is evaluated by presenting the plots of t_{cut}, t_{cyc}, Y^{Pr}, and Y, as detailed in cf. eqs 42−45) in Figures 11 and 12.

Figure 11 illustrates the impact of altering the starting times of the gradients for a constant gradient end time t_e = 80 min. The analysis reveals a notable increase in cut time, rising from 33.913 min at t_s = 0 to 82.1793 min when t_s reaches 70 min. Beyond this point, the cut time stabilizes, indicating no further significant changes. Similarly, the findings demonstrate a reduction in cycle time, decreasing from 95.6522 to 90.8690 min and then stabilizing after t_s = 70 min. Additionally, fluctuations in cycle time were observed in the interval between t_s = 20 and 70 min, highlighting a period of variability before stabilization. The results indicate an initial increase in productivity up to t_s = 10 min followed by a decline at t_s = 15 min. Subsequent observations show that productivity levels off, as depicted in the plot, demonstrating stabilization beyond this point. The analysis of yield plots similarly reveals consistent trends, indicating parallel observations with the previously discussed productivity results.

Figure 12 demonstrates the effects of varying the ending times of gradients while maintaining a constant start time of t_s = 5 min for these gradients. The cut time plot illustrates an initial upward trend, escalating from 47.8261 min at t_e = 5 to 53.913 min at t_e = 24 min, followed by a sharp decrease in cut time noted at t_e = 30 min. Subsequently, minor fluctuations in the cut time were observed, continuing until t_e = 80 min. The cycle time exhibits a consistent decline, moving from 103.913 min at t_e = 5 to 93.193 min by t_e = 73

https://doi.org/10.1021/acsomega.4c02444
ACS Omega 2024, 9, 20601−20615

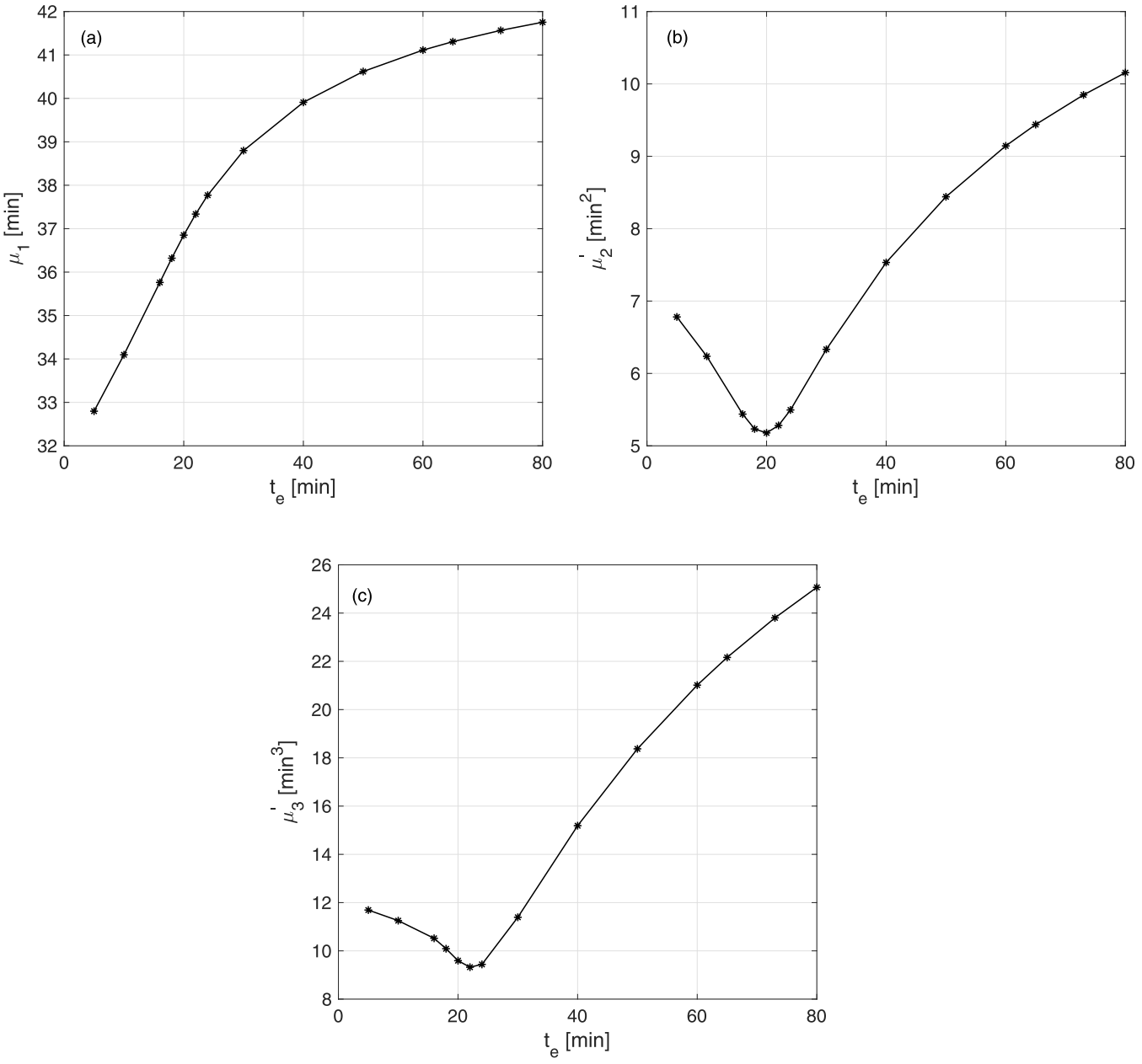

Figure 10. Effects of gradient end time on the moments for component 1 obtained by numerical integration for the LSS gradient model, considering the reference parameters given in Table 1, while t_e was gradually changed.

min. Nonetheless, within the interval from t_e = 30 min to t_e = 80 min, minor fluctuations in cycle time were detected, indicating a period of variability within this range. The productivity plot indicates a stable phase between t_e = 5 min and t_e = 24 min. Subsequently, a pronounced drop in productivity is observed at t_e = 30 min, followed by noticeable variations in productivity persisting until t_e = 80 min. The examination of yield plots unveils trends that are consistent with those observed in the productivity analysis, suggesting aligned findings across both sets of results.

7. CONCLUSIONS

A nonlinear and nonequilibrium model of gradient elution chromatography was introduced and solved numerically using an HR-FVS. The numerical approximation of the considered model is more challenging for a numerical scheme than for the model of isocratic elution chromatography. This is because the retention behaviors of the mixture components are changing in the chromatographic run with varying solvent composition. Different functional relationships among the model parameters and solvent volume fraction were considered to analyze the effects of gradient starting and ending times, modulator concentration magnitude, and gradient slope. The consideration and study of such relationships were necessary for enhancing the process efficiency and productivity as well as matching of the experimental and theoretical results. The superiority of gradient elution over isocratic elution was demonstrated through a variety of test problems, considering various operating conditions. It was observed that such techniques can play a dominant role in both analytical and preparative chromatography. The numerical results showed that the

https://doi.org/10.1021/acsomega.4c02444
ACS Omega 2024, 9, 20601−20615

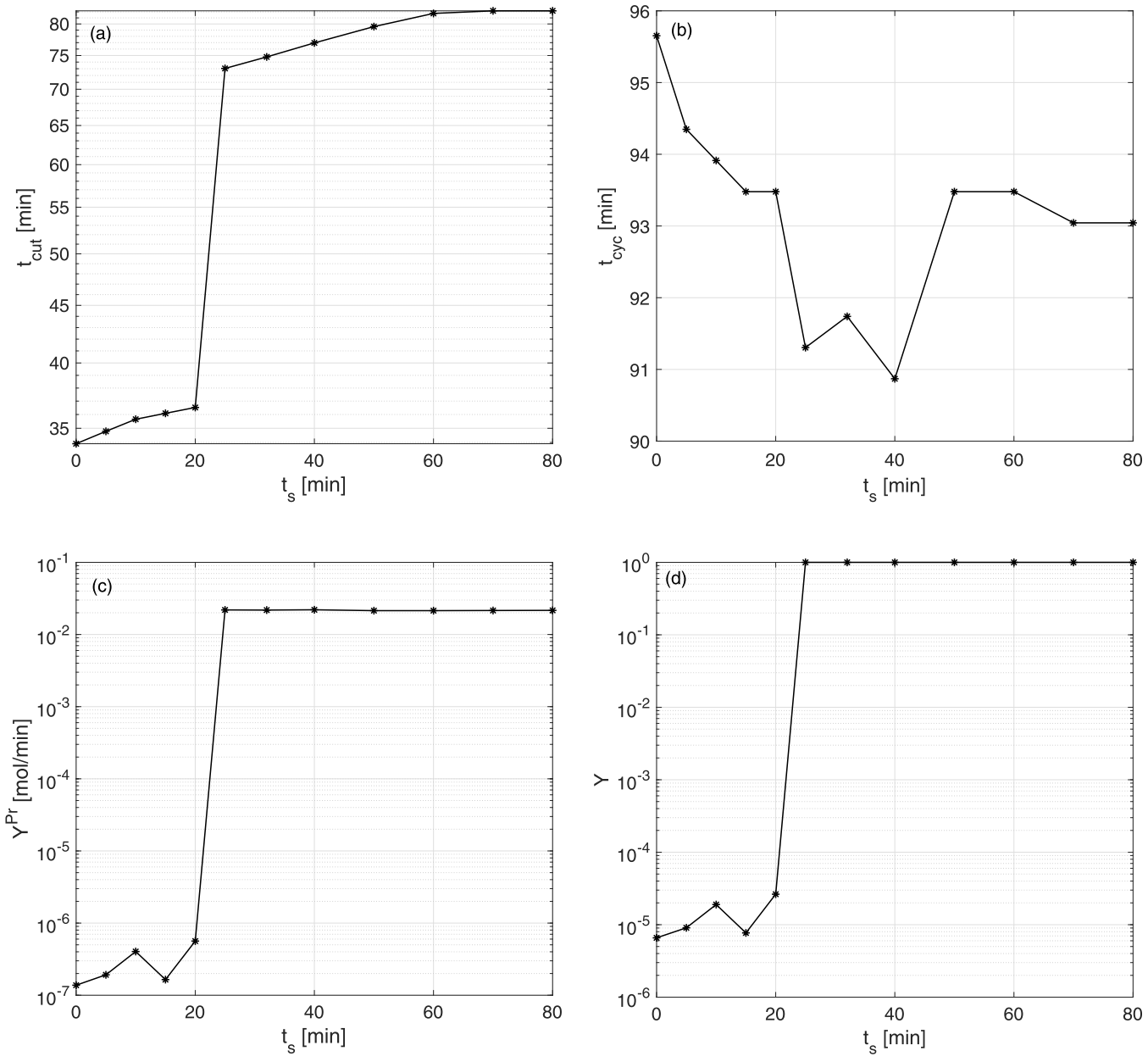

Figure 11. Plots of (a) t_{cut}, (b) t_{cyc}, (c) Y^{Pr}, and (d) Y for component 1, as a function of gradient start time t_s for LSS gradient model, considering the reference parameters given in Table 1.

gradient elution technique is extremely useful for the rapid separation of mixture components. Furthermore, conventional equipment and HPLC columns can be utilized without any difficulty. The results of this theoretical study will be helpful to upgrade and optimize the gradient elution chromatography process. Although no experimental results were available for comparison, we have provided a tool which practitioners can reuse according to their own experimental conditions.

AUTHOR INFORMATION

Corresponding Author

Sadia Perveen − *Department of Mathematics, COMSATS University, Islamabad 45550, Pakistan; Department of Mathematics, Air University, Islamabad 44230, Pakistan;* orcid.org/0000-0001-8098-6727; Phone: +92 3215959377; Email: sadia.ahsan@au.edu.pk

Authors

Arif Mahmood − *Department of Mathematics, COMSATS University, Islamabad 45550, Pakistan*

Muhammad Uzair − *Department of Mathematics, COMSATS University, Islamabad 45550, Pakistan*

Nazia Rehman − *Department of Mathematics, COMSATS University, Islamabad 45550, Pakistan;* orcid.org/0000-0003-0063-1454

Shamsul Qamar − *Department of Mathematics, COMSATS University, Islamabad 45550, Pakistan;* orcid.org/0000-0002-7358-6669

Complete contact information is available at: https://pubs.acs.org/10.1021/acsomega.4c02444

Funding

The authors have not received any grants for the current research work from their respective institutions.

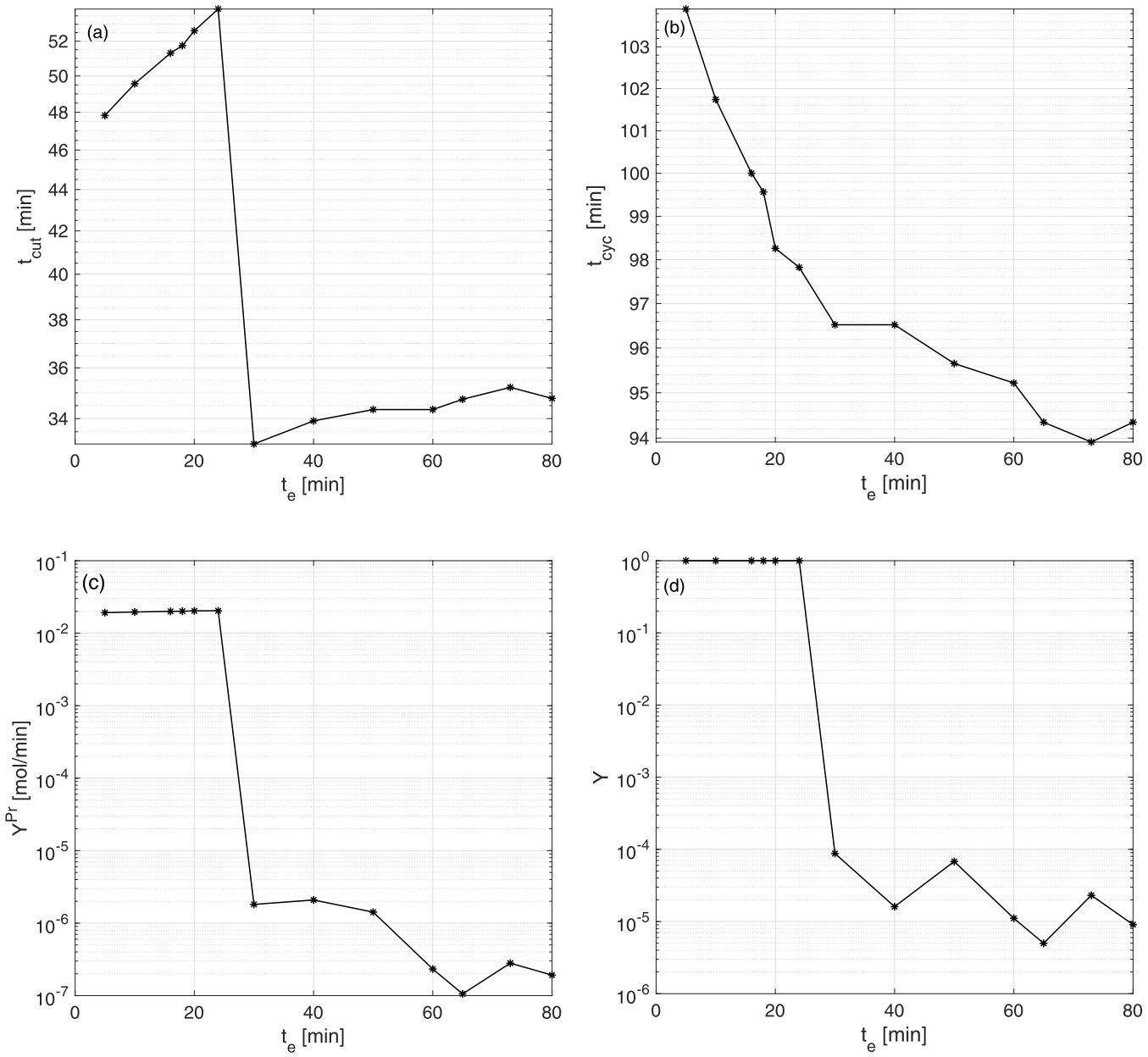

Figure 12. Plots of (a) t_{cut}, (b) t_{cyc}, (c) Y^{Pr}, and (d) Y for component 1, as a function of gradient end time t_e for the LSS gradient model, considering the reference parameters given in Table 1.

Notes

The authors declare no competing financial interest.

■ ACKNOWLEDGMENTS

We thank the anonymous referees for their useful suggestions.

■ REFERENCES

(1) Jandera, P.; Churacek, J. *Gradient Elution in Column Liquid Chromatography*; Elsevier: Amsterdam, 1985.

(2) Snyder, L. R. *High Performance Liquid Chromatography-Advances and Perspectives*; Horvath, C., Ed.; Wiley: New York, NY, 1986; Vol. 1.

(3) Snyder, L. R.; Dolan, J. *High Performance Gradient Elution-The Particle Application of the Linear Solvent-Strength Model*; Wiley & Sons: Hoboken, 2007.

(4) Poppe, H.; Paanakker, J.; Bronckhorst, M. Peak width in solvent-programmed chromatography: I. General description of peak broadening in solvent-programmed elution. *J. Chromatogr.* **1981**, *204*, 77−84.

(5) Guiochon, G.; Lin, B. *Modelling for Preparative Chromatography*; Academic Press: Amsterdam, 2003.

(6) Jandera, P. Gradient elution in liquid column chromatography-prediction of retention and optimization of separation. In *Advances in Chromatography*; CRC Press, 2004; Vol. *43*, pp 1−108.

(7) Hao, W.; Di, B.; Chen, Q.; Wang, J.; Yang, Y.; Sun, X. Study of the peak variance in isocratic and gradient liquid chromatography using the transport model. *J. Chromatogr. A* **2013**, *1295*, 67−81.

(8) Donaldson, K. O.; Tulane, V. J.; Marshall, L. M. Automatically increasing solvent polarity in chromatography. *Anal. Chem.* **1952**, *24*, 185−187.

(9) Snyder, L.; Dolan, J.; Gant, J. Gradient elution in high-performance liquid chromatography. *J. Chromatogr.* **1979**, *165*, 3−30.

(10) Neue, U. D. *Gradient Elution Theory*; published on-line at Chromedia.nl, April 2007.

https://doi.org/10.1021/acsomega.4c02444
ACS Omega 2024, 9, 20601−20615

(11) Snyder, L. R.; Dolan, J. W. The linear-solvent-strength model of gradient elution. In *Advances in Chromatography*; CRC Press, 1998; Vol. *38*, pp 115−187.
(12) Snyder, L. R.; Dolan, J. W. Linear-Solvent-Strength Model of Gradient Elution. In *Advances in Chromatography*; CRC Press: Boca Raton, 2021.
(13) Baeza-Baeza, J. J.; Ortiz-Bolsico, C.; Torres-Lapasió, J.; García-Álvarez-Coque, M. Approaches to model the retention and peak profile in linear gradient reversed-phase liquid chromatography. *J. Chromatogr. A* **2013**, *1284* (1284), 28−35.
(14) Qamar, S.; Rehman, N.; Carta, G.; Seidel-Morgenstern, A. Analysis of gradient elution chromatography using the transport model. *Chem. Eng. Sci.* **2020**, *225*, 115809.
(15) Furusaki, S.; Haruguchi, E.; Nozawa, T. Separation of proteins by ion-exchange chromatography using gradient elution. *Bioprocess Eng.* **1987**, *2*, 49−53.
(16) Antia, F. D.; Horvath, C. Gradient elution in nonlinear preparative liquid chromatography. *J. Chromatogr.* **1989**, *484*, 1−27.
(17) Neue, U. D.; Phoebe, C. H.; Tran, K.; Cheng, Y. F.; Lu, Z. Dependence of reversed-phase retention of ionizable analytes on pH, concentration of organic solvent and silanol activity. *J. Chromatogr. A* **2001**, *925* (1−2), 49−67.
(18) Nikitas, P.; Pappa-Louisi, A.; Agrafiotou, P. Effect of the organic modifier concentration on the retention in reversed-phase liquid chromatography. *J. Chromatogr. A* **2002**, *946* (1−2), 33−45.
(19) Torres-Lapasio, J. R.; Garcia-Alvarez-Coque, M. C.; Bosch, E.; Roses, M. Considerations on the modelling and optimisation of resolution of ionisable compounds in extended pH-range columns. *J. Chromatogr. A* **2005**, *1089* (1−2), 170−186.
(20) Lazaro, E.; Izquierdo, P.; Rafols, C.; Roses, M.; Bosch, E. Prediction of retention in reversed-phase liquid chromatography by means of the polarity parameter model. *J. Chromatogr. A* **2009**, *1216* (27), 5214−5227.
(21) Tellez, A.; Roses, M.; Bosch, E. Modeling the Retention of Neutral Compounds in Gradient Elution RP-HPLC by Means of Polarity Parameter Models. *Anal. Chem.* **2009**, *81* (21), 9135−9145.
(22) Vivo-Truyols, G.; Torres-Lapasio, J. R.; García-Alvarez-Coque, M. Error analysis and performance of different retention models in the transference of data from/to isocratic/gradient elution. *J. Chromatogr. A* **2003**, *1018* (2), 169−181.
(23) Nikitas, P.; Pappa-Louisi, A.; Agrafiotou, P. Effect of the organic modifier concentration on the retention in reversed-phase liquid chromatography: I. General semi-thermodynamic treatment for adsorption and partition mechanisms. *J. Chromatogr. A* **2002**, *946* (1−2), 9−32.
(24) Nikitas, P.; Pappa-Louisi, A. Retention models for isocratic and gradient elution in reversed-phase liquid chromatography. *J. Chromatogr. A* **2009**, *1216* (10), 1737−1755.
(25) Neue, U. D. Nonlinear Retention Relationships in Reversed-Phase Chromatography. *Chromatographia* **2006**, *63*, S45−S53.
(26) Neue, U. D.; Kuss, H. Improved reversed-phase gradient retention modeling. *J. Chromatogr. A* **2010**, *1217*, 3794−3803.
(27) Qamar, S.; Warnecke, G. A high-order kinetic flux-splitting method for the relativistic magnetohydrodynamics. *J. Comput. Phys.* **2005**, *205*, 182−204.
(28) Qamar, S.; Warnecke, G. A space-time conservative method for hyperbolic systems with stiff and non-stiff source terms. *Commun. Comput. Phys.* **2006**, *1*, 449−478.
(29) Qamar, S. Modeling and simulation of population balances for particulate processes. Habilitation Thesis, Faculty of Mathematics, OVGU, Magdeburg, Germany, 2008.
(30) Koren, B. *A Robust Upwind Discretization Method for Advection, Diffusion and Source Terms*; Centrum voor Wiskunde en Informatica: Amsterdam, 1993; pp 117−138.
(31) Pietrzak, J. The use of TVD limiters for forward-in-time upstream-biased advection schemes in ocean modeling. *Mon. Weather Rev.* **1998**, *126*, 812−830.
(32) Horvath, K.; Felinger, A. Influence of Particle Size and Shell Thickness of Core-shell Packing Materials on Optimum Experimental Conditions in Preparative Chromatography. *J. Chromatogr. A* **2015**, *1407*, 100−105.
(33) Debets, H. J. G.; Bajema, B. L.; Doornbos, D. A. A critical evaluation of quality criteria for the optimization of chromatographic multicomponent separations. *Anal. Chim. Acta* **1983**, *151*, 131−141.

https://doi.org/10.1021/acsomega.4c02444
ACS Omega 2024, 9, 20601−20615